

Small-Scale Convective Instability and Upper Mantle Viscosity Under California

George Zandt and Charles R. Carrigan

Thermal calculations and convection analysis, constrained by seismic tomography results, suggest that a small-scale convective instability developed in the upper 200 kilometers of the mantle under California after the upwelling and cooling of asthenosphere into the slab window associated with the formation of the San Andreas transform boundary. The upper bound for the upper mantle viscosity in the slab window, 5×10^{19} pascal seconds, is similar to independent estimates for the asthenosphere beneath young oceanic and tectonically active continental regions. These model calculations suggest that many tectonically active continental regions characterized by low upper mantle seismic velocities may be affected by time-dependent small-scale convection that can generate localized areas of uplift and subsidence.

The possible presence and influence of small-scale upper mantle convection in oceanic and tectonically active continental regions is uncertain (1–3). Seismic tomography is providing direct evidence on global patterns of mantle convection (4, 5), but high-resolution images are required for the investigation of small-scale convection in the upper mantle. We used tomographic results from central California and tectonic data on the slab window that developed after formation of the San Andreas fault system to characterize the cooling of the new mantle. Along with an analytical model of the instability of the cooling mantle, these observations and constraints provide an estimate for the upper mantle viscosity under California.

Until about 30 million years ago (Ma), the entire western coastline of California was the site of subduction of the oceanic Farallon plate. At this time, a section of the Pacific-Farallon spreading center began to be consumed under the North American plate as the San Andreas fault, a new transform boundary, formed (Fig. 1) (6, 7). Adjacent to the new transform boundary, a slab window (upper mantle space that was previously occupied by a subducting plate) opened under southern California and lengthened northward during the past 25 to 30 million years (8). In the slab window, upwelling asthenosphere replaced the sinking remnants of the Farallon plate and influenced the tectonics of coastal California (9).

Recent seismic tomography results obtained by several independent groups using different techniques (linearized inversion and back-projection) provide coverage of the upper mantle *P*-wave velocity variations under California to depths of ~250 km; the average spatial resolution is ~50 km (10–13). The results (Fig. 2) show the

presence of a deep high-velocity (>3%) anomaly north of Cape Mendocino, consistent with subduction of the Gorda plate under the North American plate there (11). A second, enigmatic deep region of high velocity underlies the southern Great Valley (SGV) to a depth of 230 km (12–16). This anomaly is separate from but similar to another high-velocity anomaly under the Transverse Ranges, which was interpreted as downwelling of converging subcrustal lithosphere (15, 17). The local convergence was related to the major westward step in the San Andreas fault at the big bend. Such a model cannot be used to explain the SGV anomaly, however, because it is not located in a region of convergence.

The opening of the slab window under California provides a natural convection experiment. Hot upper mantle material was suddenly emplaced at the base of a relatively cold, thin lithosphere. We assume that the new mantle cools conductively until the thermal boundary layer between the chilled lithosphere and asthenosphere reaches a critical thickness; then the cool, dense mantle becomes unstable, detaches, and sinks (Fig. 3). The sinking mantle induces an upward counterflow of warm mantle. This interpretation differs from

that of the Transverse Range anomaly (15, 17) because the high-velocity cool body is interpreted as dripping off the base of the lithosphere (16) instead of a being driven downward by the subduction of subcrustal lithosphere. We evaluate this model using reasonable values for upper mantle properties beneath California and boundary conditions provided by the tectonic history. The time constraints are the opening of the slab window at the latitude of the Great Valley and the time required for the cool mantle to sink to the depth observed from tomography. The diameter of the mantle blob provides a constraint on the estimated maximum thickness of the thermal boundary layer before it became unstable.

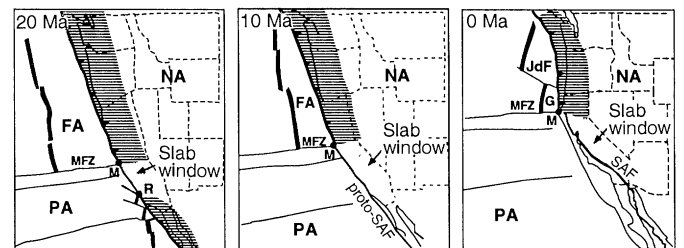
As the thermal boundary layer forms, the increasing thickness of higher density mantle will destabilize the lower portion of the layer. The local Rayleigh number (18, 19) is

$$(Ra)^* = \alpha g \Delta T \delta^3 \rho / \kappa \mu \quad (1)$$

where α is the coefficient of thermal expansion ($2 \times 10^{-5} \text{ K}^{-1}$), g is the gravitational acceleration (10 m s^{-2}), ρ is density (3700 kg m^{-3}), κ is thermal diffusivity ($1.5 \times 10^{-6} \text{ m}^2 \text{ s}^{-1}$), ΔT is the temperature drop across a boundary layer of thickness δ , and μ is the dynamic viscosity. When $(Ra)^*$ reaches a critical value of about 1000, the layer of thickness δ becomes unstable and sinks as a blob in a time period small compared with the time for the development of the instability (Fig. 3) (18). The calculation of the thickness and temperature difference across the boundary layer requires some assumptions about the temperature-dependent rheology of the mantle. We follow Parsons and McKenzie (1) and pick an isotherm of 975°C to represent the transition from rigid to viscous behavior. Then ΔT is measured from the 975°C isotherm to another isotherm of γT , where T is the uniform temperature of the interior mantle and γ is a constant near 1. We assume $T = 1300^\circ\text{C}$ and $\gamma = 0.97$, which makes $\Delta T = 286^\circ\text{C}$.

To examine the growth of the boundary

Fig. 1. Plate reconstructions showing the relative plate motions of the North American (NA), Farallon (FA), and Pacific (PA) plates over the past 20 million years. After 10 Ma, the Farallon plate broke into the smaller Juan de Fuca (JdF) and Gorda (G) plates. The Mendocino (M) and Rivera (R) triple junctions and the Mendocino fault zone (MFZ) are shown. The shallow, subhorizontal portion of the subducting plate is outlined with horizontal lines, and the shallow slab window is outlined with stippling. Heavy solid lines are oceanic ridges; heavy line with barbs is subduction zone; solid lines are faults [including San Andreas (SAF)]; and dashed lines show state boundaries and indicate internal deformation of NA plate. [Adapted from (7)]



the shallow, subhorizontal portion of the subducting plate is outlined with horizontal lines, and the shallow slab window is outlined with stippling. Heavy solid lines are oceanic ridges; heavy line with barbs is subduction zone; solid lines are faults [including San Andreas (SAF)]; and dashed lines show state boundaries and indicate internal deformation of NA plate. [Adapted from (7)]

Institute of Geophysics and Planetary Physics, Earth Sciences Division, L-202, Lawrence Livermore National Laboratory, Livermore, CA 94550.

layer, we solved the one-dimensional heat conduction equation (20) with initial conditions for an isothermal asthenosphere (1300°C) emplaced at the base of a 50-km-thick conductive lithosphere with an initial $12^{\circ}\text{C km}^{-1}$ geothermal gradient appropriate for a subduction zone (Fig. 4). The growth of the thermal boundary layer follows the relation,

$$\delta = c(\kappa t)^{1/2} \quad (2)$$

where the constant $c = 1.5$ for our boundary conditions.

The most uncertain parameter in Eq. 1 is the viscosity. Therefore, we used Eqs. 1 and 2 to calculate the viscosity required to produce an instability in a given time (Table 1). The results show a range of viscosities between 3×10^{18} and 3×10^{19} Pa s for times between 5 and 25 My.

The uncertainty of the instability criterion raises the question of the precise meaning of the critical time for the development of the instability—is it the initiation time or does it include some partial development of the blob—and the sensitivity of the results to variations in boundary conditions. Some of these issues were addressed in a numerical study of two-dimensional transient convection for the oceanic lithosphere (21). Our problem is similar to the cooling of oceanic lithosphere except we start with a lithosphere of finite thickness. In the numerical study (21), the onset time (t_0) was defined as when the amplitude of convection had grown by an order of magnitude and cold thermals had formed. To take advantage of the numerical simulations, we calibrated our problem to the oceanic one using our calculated temperature profiles (Fig. 4). After 5

million years, the temperature profile of the slab window takes on the shape of the temperature profile for a 60-km-thick, 30-million-year-old oceanic lithosphere (this calibration is dependent on the thickness and initial temperatures of the overlying conductive layer). The thermal evolution in both problems is nearly identical after this time. Using this equivalency (22), we calculated the critical thickness and corresponding viscosity (for both free and no-slip boundary conditions) for a range of onset times (Table 1). The range of viscosity values (1×10^{18} to 5×10^{19} Pa s) brackets the range obtained with the approximate local Rayleigh number criterion.

If the SGV anomaly is a growing thermal instability, the half width of the feature corresponds to the boundary layer thickness (Fig. 3). The diameter is approximately 100 to 150 km, which gives a critical δ of approximately 50 to 75 km. The predicted thicknesses are marginally too small for the shorter onset times of 5 and 10 million years. The results for 15 to 25 million years give values for δ_c of 45 to 60 km, which are in better agreement with the seismic results and are within the geologic time constraints. The temperature contrast estimated from the seismic anomaly is consistent with a cold thermal drip, within the range of the laboratory-measured temperature dependence of seismic velocities (23). Considering both boundary conditions, our analysis places an upper bound of 5×10^{19} Pa s and a less certain lower bound of about 1×10^{18} Pa s for the upper mantle viscosity in the slab window under California.

Our calculated range of viscosities based on the local Rayleigh number is similar to estimates for an upper mantle low-viscosity layer (24–26) based on constant viscosity

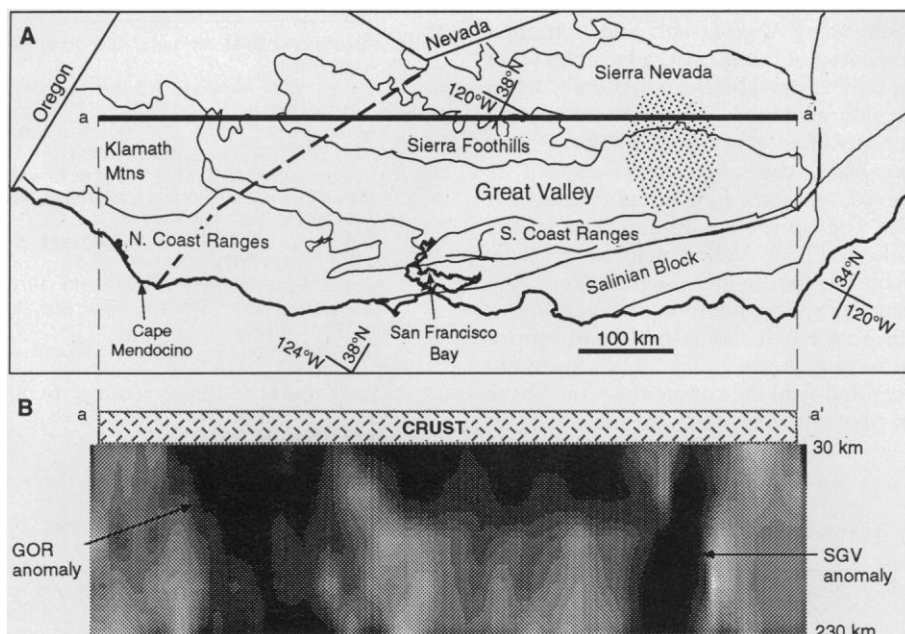


Fig. 2. Seismic P -wave velocity anomalies in upper mantle beneath California. **(A)** In map view, dark solid lines outline major geologic provinces. The stippled area in the southern Great Valley (SGV) represents the location and size of the SGV anomaly over the depth range of 150 to 190 km. Dashed line extending from Cape Mendocino to Lake Tahoe (on the California-Nevada border) marks southernmost extent of the subducting Gorda (GOR) plate. **(B)** Depth extent of high-velocity anomalies GOR and SGV in the cross section aa' from (A). Gray scale represents velocity variations from -3% (white) to $+3\%$ (black). Thus, black areas have velocities $>3\%$ higher than the background velocity [based on results from (12)].

Fig. 3. Schematic cross section of the development of an unstable thermal boundary layer and the formation of an upper mantle blob in the slab window beneath California. The steeply dipping part of the Gorda plate is the interpretation for the GOR anomaly and the sinking blob is the interpretation for the SGV anomaly. Half-arrows indicate sense of relative motion between the North American and Gorda plates.

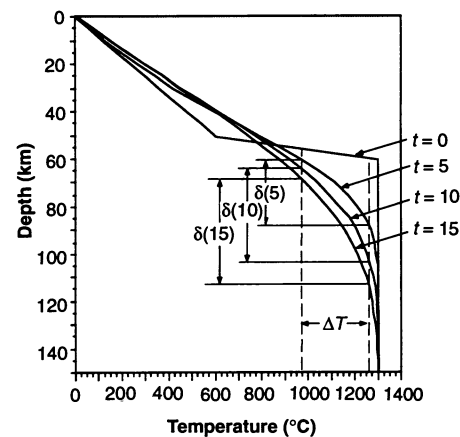
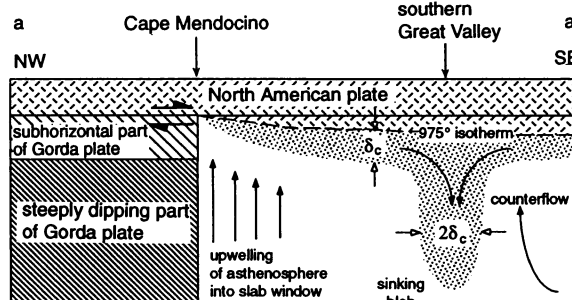


Fig. 4. Vertical temperature profiles from a conductive cooling model for times $t = 0, 5, 10,$ and 15 million years show the evolution of the temperatures in the mantle. The intersections of the temperature profiles with the 975°C and 1265°C isotherms defines the growth of the thermal boundary layer.

models for the rebound of the Pleistocene Lake Bonneville shorelines in Utah (25) and changes in lake levels in Iceland associated with load changes from a nearby ice cap (26), but the range is significantly less than the estimated average whole mantle viscosity of 10^{21} Pa s (27). Observations of linear topography and gravity anomalies under young oceanic lithosphere are consistent with convective instability in a mantle with an average viscosity of 10^{18} Pa s developing within 5 to 10 million years of the start of plate cooling (28, 29). Therefore, small-scale convection cannot explain the 70- to 80-million-years flattening of the oceanic subsidence rate (29), but other mechanisms can account for this effect (30).

Mantle viscosity is most likely temperature- and pressure-dependent (29, 31, 32). Studies of small-scale convection with variable or temperature- and pressure-dependent viscosity (2, 29, 31–33) all agree that convective instability is possible if the upper mantle viscosity is sufficiently low (about 1×10^{18} Pa s). In particular, Buck and Parmentier (29) predict instability in 5 to 10 million years for an oceanic mantle with a temperature- and pressure-dependent viscosity profile with a minimum of 1×10^{18} Pa s in the shallow asthenosphere. This result is within the range of viscosity we calculated using the simple local Rayleigh number criterion. Previous studies (28, 33) have noted that for order-of-magnitude estimates of onset time, the local Rayleigh number criterion is robust, even in comparison with variable viscosity calculations.

In a global upper mantle tomography study (5), shear velocity variations of $\pm 4\%$ were mapped at depths of 100 to 200 km, which implies that the upper mantle is characterized by large domains of high temperatures and the asthenosphere is not homogeneous. The regions with evidence for low upper mantle viscosity—California, Utah, Iceland, east-central Pacific Ocean, and southern Indian Ocean—are characterized by slow upper mantle velocities. From

this correlation, we infer that other regions characterized by slow upper mantle velocities—such as the western United States, central America, southwest Pacific, southeast Asia, northeastern Africa, western Europe, and Siberia-Alaska—are potential sites of unstable boundary layers and small-scale convection in the upper mantle. If small-scale convection is ubiquitous over large domains of the Earth, the process will have important implications for estimates of global heat loss (34).

We must also consider the effect, if any, that shallow mantle flow has on the overlying crust. The flow's dynamical stresses on the elastic layer will generate topography variations as large as 1 km with lows centered on the downwelling sites (20, 31). If the overlying plate is strong and intact, a downward flexure will form, creating a sedimentary basin on the surface (Fig. 5A). On the other hand, if the plate is weak or broken along a weak fault and horizontal compressional forces exist, a localized uplift can result (Fig. 5B). In either case, when the blob eventually breaks free from the boundary layer, abruptly thinning the overlying plate, the subcrustal forces will be relieved, and some form of uplift will occur (32). The convective instability under the southern Great Valley may be partially responsible for the increase in tectonic subsidence of the southern San Joaquin Valley basin that began about 16 Ma and continues to the present (35). The downward forces and flanking counterflows may have contributed to the westward tilt and uplift

of the adjacent southern Sierra Nevada mountains (Fig. 5A). Farther south, perhaps another mantle downwelling occurs beneath the San Andreas fault, and the surface manifestation is the compressional Transverse Ranges astride the big bend in the San Andreas fault. Kinematic modeling cannot distinguish whether downwelling caused the big bend in the San Andreas or if the big bend induced the local subduction in the mantle (15). In the case of the southern Great Valley anomaly, it is difficult to envision a mechanism by which the 200-km-deep mantle blob is a consequence of crustal convergence. On the other hand, if the mantle flows are primary (once initiated by the opening of the slab window), both the SGV and Transverse Range anomalies and their disparate surface manifestations can be explained.

REFERENCES AND NOTES

1. B. Parsons and D. McKenzie, *J. Geophys. Res.* **83**, 4485 (1978).
2. D. A. Yuen, W. R. Peltier, G. Schubert, *Geophys. J. R. Astron. Soc.* **65**, 171 (1981).
3. L. I. Makeyeva, L. P. Vinnik, S. W. Roecker, *Nature* **358**, 144 (1992); P. Molnar, *ibid.*, p. 105.
4. B. H. Hager and R. W. Clayton, in *Mantle Convection*, W. R. Peltier, Ed. (Gordon and Breach, New York, 1989), pp. 657–764.
5. D. L. Anderson, T. Tanimoto, Y.-S. Zhang, *Science* **256**, 1645 (1992).
6. T. Atwater, *Geol. Soc. Am. Bull.* **81**, 3513 (1970).
7. J. Severinghaus and T. Atwater, *Geol. Soc. Am. Mem.* **176**, 1 (1990).
8. W. R. Dickinson and W. S. Snyder, *J. Geol.* **87**, 609 (1979).
9. G. Zandt and K. P. Furlong, *Geology* **10**, 376 (1982); K. P. Furlong, W. D. Hugo, G. Zandt, *J. Geophys. Res.* **94**, 3100 (1989); M. Liu and K. P. Furlong, *ibid.* **97**, 4941 (1992).
10. E. D. Humphreys and R. W. Clayton, *J. Geophys. Res.* **95**, 19725 (1990).
11. H. M. Benz, G. Zandt, D. H. Oppenheimer, *ibid.* **97**, 4791 (1992).
12. H. M. Benz and G. Zandt, in *Seismic Tomography*, H. M. Iyer and K. Hirahara, Ed. (Chapman and Hall, London, in press). In this report, the SGV anomaly was interpreted as one of several remnant fragments of a subducting and fragmenting Farallon plate. The persistence of the anomaly over periods of 20 My was attributed to compositional differences or anisotropy that persists beyond the time required for thermal equilibration.
13. G. P. Biasi and E. D. Humphreys, *Geophys. Res. Lett.* **19**, 1161 (1992).
14. K. Aki, *Rev. Geophys. Space Phys.* **20**, 161 (1982). Aki reviewed seismic tomography results for California available at the time and made some inferences about flow in the asthenosphere. On the basis of an interpretation of the low-velocity zone under central California as the preserved shape of the downgoing slab that has persisted for up to 10 million years, Aki suggested the mantle flow rate is 10^{-3} m year⁻¹. Such slow flow rates required relatively small density variations corresponding to the velocity variations that were consistent with low velocities caused by melts in penny-shaped cracks with small aspect ratios. The more recent tomography results show that the slab shape of the low-velocity zone is preserved but only to depths of 100 to 150 km. To those depths, the preserved shape can be explained by the rigidity of the North American lithosphere, the base of which must mirror the shape of the extinct slab.
15. E. D. Humphreys and B. H. Hager, *J. Geophys. Res.* **95**, 19747 (1990).

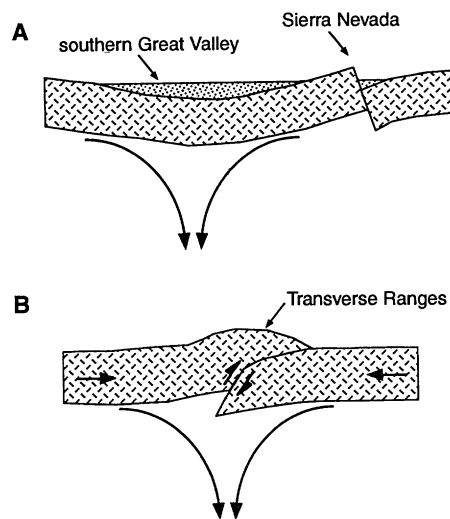


Fig. 5. Schematic drawings of the geologic consequences of the interaction of an upper mantle downwelling current with an overlying plate. (A) In the case of a strong plate, the dynamic forces induced by the convection causes a downward flexure with a depositional basin at the surface. (B) In the case of a weak or broken plate, compressional forces can produce a localized uplift.

Table 1. Calculated critical thickness δ and dynamic viscosity of the boundary layer for a prescribed instability onset time t . The calculated viscosities are based on the local Rayleigh number criterion (from Eq. 1) and on the equivalency to numerical models with no-slip and free boundary conditions (bc). My, million years.

t (My)	δ (km)	Viscosity (10^{18} Pa s)		
		Eq. 1	No-slip bc	Free bc
5	28.5	3.3	1.3	4.0
10	38.7	8.2	3.8	12
15	45.5	13	7.0	22
20	52.0	20	11	34
25	57.5	27	15	48

16. C. H. Jones, H. Kanamori, S. W. Roecker, *ibid.*, in press.
17. P. Bird and R. W. Rosenstock, *Geol. Soc. Am. Bull.* **95**, 946 (1984).
18. L. N. Howard, in *Proceedings of the 11th International Congress of Applied Mechanics, Munich, Germany, 1964*, H. Gortler, Ed. (Springer-Verlag, Berlin, 1966), p. 1109.
19. J. Elder, *The Bowels of the Earth* (Oxford Univ. Press, London, 1976); the concept of a local Rayleigh number was developed for the analysis of transient convection from a thermal boundary layer. Later experimental and numerical analysis have confirmed the general validity of this type of analysis [C. R. Carrigan, *Science* **215**, 965 (1982); (21)].
20. D. L. Turcotte and G. Schubert, *Geodynamics* (Wiley, New York, 1982).
21. G. Houseman and D. McKenzie, *Geophys. J. R. Astron. Soc.* **68**, 133 (1982).
22. The thermal evolutions in both the oceanic problem and our problem are nearly identical after 5 million years, our temperature profile taking on that of a 30-million-years-old oceanic lithosphere. We expressed this equivalency between time in our problem, t , and time in the oceanic problem, t' , with

$$t = t' - 25 \text{ million years} \quad (3)$$

where $t' > 30$ million years. The onset time for the oceanic problem of $t'_o = 90$ million years, corresponding to a viscosity of $\mu^* = 2 \times 10^{20}$ Pa s (21), is equivalent to an onset time of $t_o^* = 65$ million years in our problem. This onset time is clearly too long to satisfy the geologic time constraint. The most uncertain and variable parameter is the viscosity, so we used Eqs. 1 and 2 to relate the viscosity to onset time

$$\mu \propto \Delta T (t_o)^{3/2} \quad (4)$$

and used this relation to find the relation between ratios of viscosities and onset times

$$\mu/\mu^* = (t_o/t_o^*)^{3/2} \quad (5)$$

Using Eqs. 2 and 5, we calculated the critical thickness, δ_c , and the corresponding μ (for both free and no-slip boundary conditions) for a range of $t_o < 25$ million years (since the opening of the slab window at the latitude of the anomaly) (Table 1).

23. The estimated temperature contrast represented by the seismic anomaly provides an important distinction between a sinking thermal blob and a sinking lithospheric plate. Many studies [(15); P. M. Davis, *Tectonophysics* **197**, 309 (1991)] have used values for the temperature dependence of compressional velocity, $\partial V_p/\partial T$, of $-0.5 \text{ m s}^{-1} \text{ }^\circ\text{C}^{-1}$ [O. L. Anderson, E. Schreiber, R. C. Liebermann, N. Soga, *Rev. Geophys.* **6**, 491 (1968)]; temperature derivatives for aggregates are based on various theoretical models combined with single mineral laboratory measurements]. Such values imply that a 1% velocity anomaly in the upper mantle corresponds to a 160°C temperature contrast. However, recent experimental data for peridotite gives a value of $\partial V_p/\partial T$ of $-2.9 \text{ m s}^{-1} \text{ }^\circ\text{C}^{-1}$ for temperatures from 1040° to 1300°C , corresponding to those in our problem [H. Sato, I. S. Sacks, T. Murase, *J. Geophys. Res.* **94**, 5689 (1989)]. For this temperature derivative, a 1% velocity anomaly corresponds to only a 28°C temperature contrast. If we consider the smoothing effect in the seismic tomography, the observed magnitude of the SGV anomaly of about 5% is a minimum estimate, and hence we estimate that the corresponding temperature variation is 150° to 200°C . This estimate is somewhat low but consistent with the upper bound of ΔT of the predicted temperature contrast of a sinking thermal blob (288°C in our model). It is also within the range of temperature contrast, about 200° to 300°C , of sinking thermal sheets in the numerical models of boundary layer instability (21). Values of $\partial V_p/\partial T$ intermediate between the end-members cited here can be accommodated in our hypothesis if the interior mantle temperature is increased and the transition temperature from viscous to rigid behavior is decreased; these effects increase ΔT by up to a factor of 2. However, if ΔT associated with the SGV anomaly is significantly greater than 500° to

- 600°C , it supports the idea that it represents delamination of a cold lower lithosphere as opposed to the instability of a thermal boundary layer.
24. L. M. Cathles III, *The Viscosity of the Earth's Mantle* (Princeton Univ. Press, Princeton, NJ, 1975).
25. Q. R. Passey, *J. Geophys. Res.* **86**, 11701 (1981).
26. F. Sigmundsson and P. Einarsson, *Geophys. Res. Lett.* **19**, 2123 (1992).
27. W. R. Peltier, in (4), pp. 389–478.
28. W. F. Haxby and J. K. Weisell, *J. Geophys. Res.* **91**, 3507 (1986).
29. W. R. Buck and E. M. Parmentier, *ibid.*, p. 1961.
30. J. Phipps Morgan and W. H. F. Smith, *Nature* **359**, 524 (1992).
31. L. Fleitout and D. A. Yuen, *J. Geophys. Res.* **89**, 9227 (1984).
32. D. A. Yuen and L. Fleitout, *Nature* **313**, 125 (1985).
33. C. Jaupart and B. Parsons, *Phys. Earth Planet. Inter.* **39**, 14 (1985).
34. G. T. Jarvis, *ibid.* **36**, 305 (1984); G. F. Davies, *Geology* **20**, 963 (1992).
35. M. S. Rentschler and R. B. Bloch, in *Studies of the*

Geology of the San Joaquin Basin, S. A. Graham and H. C. Olsen, Eds. [Pacific Section of SEPM (Society for Sedimentary Geology), Tulsa, OK, 1988], pp. 29–52.

36. We thank A. Kersting, S. L. Beck, P. M. Davis, G. Schubert, and E. D. Humphreys for comments on an early draft; E. D. Humphreys, K. G. Dueker, C. H. Jones, H. Kanamori, and S. W. Roecker for sharing preprints; and J. Sweeney and J. Phipps Morgan for referring us to important references. We also thank the reviewers and editor for help in focusing our arguments. This research was supported by laboratory-directed research and development funds to the Institute of Geophysics and Planetary Physics at Lawrence Livermore National Laboratory (LLNL) and the Geoscience Research Program in the Department of Energy (DOE) Office of Basic Energy Sciences. This work was done under the auspices of the U.S. DOE by the LLNL under contract W-7405-ENG-48.

19 January 1993; accepted 20 May 1993

Transcription Factor TFIIIB Sites Important for Interaction with Promoter-Bound TFIID

Shinya Yamashita,* Koji Hisatake, Tetsuro Kokubo, Katsumi Doi,† Robert G. Roeder, Masami Horikoshi, Yoshihiro Nakatani,‡

Transcription initiation factor TFIIIB recruits RNA polymerase II to the promoter subsequent to interaction with a preformed TFIID-promoter complex. The domains of TFIIIB required for binding to the TFIID-promoter complex and for transcription initiation have been determined. The carboxyl-terminal two-thirds of TFIIIB, which contains two direct repeats and two basic residue repeats, is sufficient for interaction with the TFIID-promoter complex. An extra 84-residue amino-terminal region, with no obvious known structural motifs, is required for basal transcription activity. Basic residues within the second basic repeat of TFIIIB are necessary for stable interaction with the TFIID-promoter complex, whereas the basic character of the first basic repeat is not. Functional roles of other potential structural motifs are discussed in light of the present study.

Transcription of eukaryotic protein-encoding genes requires at least five general transcription initiation factors (TFIIIB, TFIID, TFIIE, TFIIIF, and TFIIH) in addition to RNA polymerase II (1). The first step in preinitiation complex formation involves TFIID binding to the TATA box in the promoter region, a process that may be facilitated by TFIIA. Subsequently, TFIIIB binds to the TFIID-promoter complex and acts as a bridging factor to incorporate RNA polymerase

II into the complex and to specify the transcription initiation site (2). It has been proposed that TFIIIB (3), as well as TFIID (1), are targets for the acidic activation domain on the transcriptional activator VP16. Therefore, exploring the mechanism by which TFIIIB interacts with the TFIID-promoter complex is necessary for understanding transcription initiation and regulation.

The isolation and characterization of cDNAs encoding TFIIIB from human (4), *Xenopus* (5), yeast (2), and *Drosophila* (6, 7) showed that TFIIIB contains a Zn(II)-finger, imperfect direct repeats, bacterial σ -factor sequence similarities, and basic repeats. To understand the functional significance of these structural motifs, we constructed a series of TFIIIB mutants and tested each mutant for basal transcription activity and the ability to interact with the TFIID-promoter complex.

A series of NH_2 -terminal deletions were constructed (Fig. 1A) (8) and the ability of the mutant proteins (Fig. 1D) (9) to support basal transcription was tested in a TFIIIB-dependent reconstituted transcription sys-

S. Yamashita, T. Kokubo, Y. Nakatani, National Institute of Neurological Diseases and Stroke, National Institutes of Health, Bethesda, MD 20892.

K. Hisatake and R. G. Roeder, Laboratory of Biochemistry and Molecular Biology, Rockefeller University, NY 10021.

K. Doi, Laboratory of Neurochemistry, NIDCD, National Institutes of Health, Bethesda, MD 20892.

M. Horikoshi, Laboratory of Biochemistry and Molecular Biology, Rockefeller University, NY 10021, and Institute of Applied Microbiology, University of Tokyo, Bunkyo-ku, Tokyo 113, Japan.

*Present address: Central Research Laboratory, Nippon Suisan Kaisha Ltd., Hachioji, Tokyo 192, Japan.

†Present address: Department of Otolaryngology, Osaka University Medical School, Osaka 553, Japan.

‡To whom correspondence should be addressed.